

Numerical Simulation of Stress-Oxidation Damage in C/SiC Composites at High Temperatures

Chen Guoqing[1], Yao Leijiang[2*], Li Bin[2], Tong Xiaoyan[2]

[1] School of Aeronautics, Northwestern Polytechnical University, Xi'an, 710072, China
[2] Institute of No. 365, Northwestern Polytechnical University, Xi'an, 710072, China

Abstract

C/SiC ceramic matrix composites are widely used in the aerospace industry due to their excellent high-temperature mechanical properties; however, stress-oxidation damage in thermo-mechanical-oxidative environments is the primary mode of material failure. Given the high cost of experimental studies and the difficulty of some existing numerical models in accurately reflecting the material's microstructure and defects, this paper proposes a representative volume element (RVE)-based finite element analysis (FEA) model to investigate the stress-oxidation damage behavior of 2D C/SiC composites. The model incorporates the material's actual microstructure and introduces initial coating cracks based on defect data measured by scanning electron microscopy (SEM). Additionally, oxidation-damage variables for the fiber bundles were defined in the model based on gas-diffusion mechanisms and carbon-fiber oxidation kinetics. By coupling mechanical stress failure with fiber bundle oxidation damage, this study numerically simulated the fracture life and residual strength of the material under different temperatures, stress levels, and oxidation times. The simulation results showed good agreement with the experimental data, validating the model's reliability. The results indicate that both increased temperature and prolonged oxidation time accelerate the kinetic reactions of carbon fibers, leading to significant depletion of the fiber bundles and, consequently, a marked decrease in the material's residual strength. At lower temperatures or shorter oxidation times, stress is the primary cause of material failure; however, under prolonged oxidation conditions, the oxidative degradation of carbon fibers becomes the dominant factor controlling macroscopic material failure. The analytical method established in this study can effectively simulate the mechanical behavior of ceramic matrix composites under stress-oxidation conditions, providing a numerical evaluation tool for in-depth investigation of the competition between diffusion and oxidation, as well as for predicting material performance.

Keywords: C/SiC; Stress Oxidation; Numerical Simulation; Residual Strength

1. Introduction

C/SiC ceramic matrix composites have emerged as crucial candidate materials for thermal structures in hypersonic vehicles and hot-end components of aero-engines, attributed to their exceptional high-temperature mechanical properties[1], high specific strength[2, 3], and superior damage tolerance[4, 5]. Furthermore, these composites demonstrate remarkable ablation resistance[6] and thermal protection performance[7] in oxidizing and ablative environments. However, when subjected to harsh thermomechanical coupling conditions[8], not only does thermomechanical coupling behavior, characterized by the interplay of thermal and mechanical properties, manifest, but it also reacts with oxidizing environments, such as oxygen, leading to pronounced chemical-thermal-mechanical coupling damage, termed Stress-Oxidation. Stress-oxidation damage is the predominant failure mode in C/SiC as a thermal structural material. In recent years, international experts and scholars have primarily investigated the stress-oxidation damage behavior of C/SiC composites through a synergistic approach that combines theoretical and experimental exploration with numerical simulation. The Halbig team conducted combined thermogravimetric and stress-oxidation experiments, revealing that the oxidation of continuous carbon fibers follows a two-stage kinetic process governed by both chemical reaction and diffusion mechanisms. In unloaded C/SiC, the "two-stage" characteristics are masked by the closure of matrix microcracks, highlighting the self-

sealing/self-protective nature of the SiC matrix. Conversely, in stress-oxidation experiments, external loading opens manufacturing defects and microcracks, facilitating oxygen ingress. Consequently, the two-stage kinetics re-emerge, resulting in accelerated fiber degradation and a marked reduction in service life[9, 10].

In the realm of experimental investigation, advancements in scientific and technological methodologies have propelled research from rudimentary stress-oxidation mechanical tests to sophisticated multi-device, synchronous, in-situ stress-oxidation damage analysis tests. Song Yingdong's team examined the stress oxidation behavior of two-dimensional SiC/BN/SiC materials at varying temperatures in air, establishing a quantitative correlation among "stress level, fracture life, and oxidation degree"[11, 12]. Meng devised a stress oxidation test system that, by integrating a high-speed camera and digital image correlation (DIC) technology outside the transparent window of an environmental chamber, facilitated in-situ tensile testing of materials while concurrently measuring full-field in-plane strain and crack initiation sites via DIC. By contrasting the disparities in curves and fracture surfaces under inert Ar and oxidizing conditions, and by employing SEM to analyze interface oxidation and variations in fiber pull-out length, the team qualitatively delineated the coupled oxidation-mechanical behavior [13]. Fang Daining's team combined synchrotron radiation X-ray microcomputed tomography (SR-μCT) with in situ experiments to simulate thermal-mechanical-oxidation coupling conditions in air at room temperature and 1650°C, elucidating the internal microstructure and damage evolution of C/SiC composites under diverse loading conditions. Simultaneously, the digital volume correlation (DVC) method was employed to quantitatively assess the three-dimensional strain field within the material during in-situ loading[14].

In the domain of numerical simulation, the focus has shifted from rudimentary macroscopic lifespan prediction to comprehensive simulations encompassing multi-field coupling, multi-scale analysis, and mesoscale failure process simulation. Mei formulated a macroscopic stress oxidation model and introduced a failure criterion to forecast material lifespan. The model employs crack opening displacement as a pivotal parameter for numerical computations, with experimental validations confirming the reliability of the predictions [15]. Song Yingdong's team developed a non-uniform oxidation model that, in conjunction with the fiber notch model, the Curtin strength model, and the BHE model, enables precise quantification of failure time and residual strength under stress-oxidation conditions. The model accounts for the influence of initial defects and coatings, scrutinizes the interplay between fiber strength and fracture ratio, and systematically evaluates the impact of oxidation time, stress, temperature, coating thickness, and fiber volume fraction on failure time and residual strength. The predictive outcomes exhibit high concordance with experimental data [16].

Currently, from an experimental standpoint, testing conditions are stringent and the associated costs substantial, rendering extensive, repetitive testing impractical and limiting the scope of experimental findings. Consequently, it becomes imperative to delve deeper into the stress-oxidation-damage behavior of materials by integrating numerical simulation methodologies. Among the extant numerical simulation techniques, some modeling approaches overly simplify the model, thereby failing to accurately replicate the material's authentic structure and morphology. In contrast, others overlook material preparation defects, impeding the faithful reproduction of the material's true damage behavior in simulation.

This paper establishes a finite element analysis (FEA) model based on the representative volume element (RVE) extracted from the periodic structure of plain-weave C/SiC. The oxidation damage variable is defined based on the diffusion mechanism of the oxidation atmosphere and the carbon fiber oxidation kinetics. This FEA model concurrently accounts for stress failure and oxidation damage in carbon fiber bundles, predicting the stress-fracture life under varying stress levels and temperatures, as well as the residual strength at different oxidation times under distinct stress levels and temperatures. The comparison between simulation results and experimental data substantiates the model's reliability, and the competitive interplay between diffusion and oxidation is explored.

2. Numerical Simulation

In the numerical simulation of the residual strength of C/SiC composites under stress-oxidation conditions, we first established a 2D RVE finite-element model incorporating coating cracks and defects. Taking into account the diffusion of oxygen through cracks and its reaction with carbon fibers,

a damage variable related to the oxidation depth was introduced to account for the reduction in fiber bundle modulus. Combining equal-strain load distribution with the Tsai-Hill/Von Mises failure criteria, the evolution of stress-oxidation damage was simulated using a VUMAT subroutine. After oxidation, the temperature was maintained at the operating temperature, and loading was continued at a constant rate until macroscopic failure of the material. The cross-sectional area ratio of the failed element was used as the criterion for overall failure, thereby yielding the material's residual strength. The flowchart is shown in *Figure 1*.

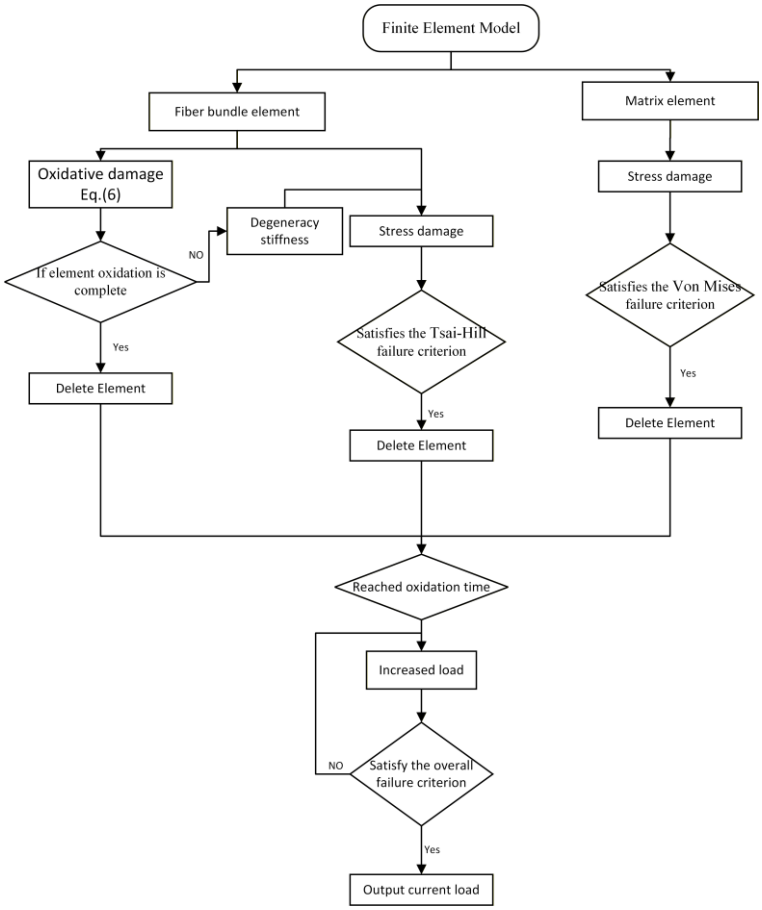


Figure 1 Flowchart for numerical simulation

2.1 RVE Model

In previous work[17], the defects and microstructure of the material were characterized using scanning electron microscopy (SEM). Based on SEM, the geometric structural parameters of the fiber bundles were determined. The curved braided structure of the fiber bundles was simplified to a wave curve equation. Then, the defect data measured in previous work were incorporated to obtain the representative volume element (RVE) model of the single-layer braided structure, as shown in *Figure 2.*

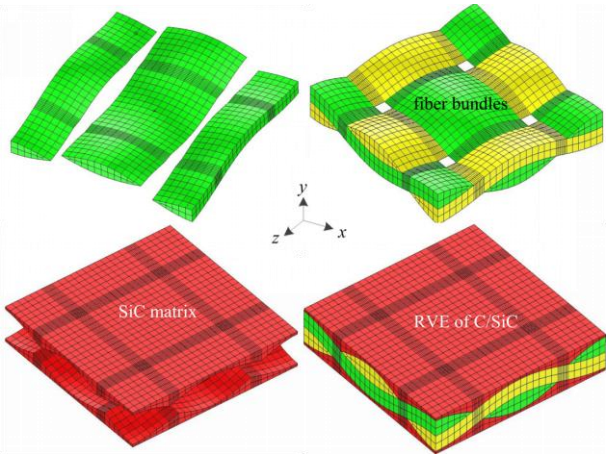


Figure 2 RVE model

In the ABAQUS/Explicit environment, using a single-layer RVE and analyzing macroscopic materials, the true material structure was considered to simulate the stress-oxidation fracture process. The specimen had 16 stacked layers. According to the principle of symmetry, this RVE model had half the thickness of the specimen, that is, 8 layers. The single-layer RVE structure was stacked, a SiC coating was applied, and relevant defects were placed based on SEM-measured defect data. Subsequently, a coating crack was prefabricated on the coating. The width of the coating crack depends on stress and temperature. Assuming that at the CVI deposition temperature (1000°C), the width of the coating crack is zero. The crack is embedded by separating the common surfaces of adjacent elements on both sides of the crack. Finally, a macroscopic material RVE model was obtained, with the model element type set to a hexahedral reduced integration element (C3D8R), comprising 100,320 elements: 42,240 fiber bundle elements, 53,280 SiC matrix elements, and 4,800 SiC coating elements. As shown in *Figure 3.*

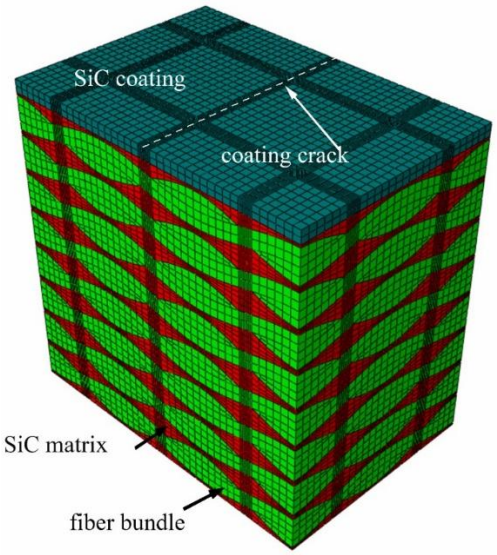


Figure 3 Finite Element Model of 2D C/SiC

Based on the characteristics of material stress oxidation behavior, the macroscopic material finite element model is divided into six different material properties, namely fiber bundle element MAT_MID_1, matrix element near the oxidation zone MAT_MID_2, matrix element outside the oxidation zone MAT_MID_3, coating element MAT_MID_4, elements on both sides of the coating crack MAT_MID_5, and MAT_MID_6.

2.2 Stress oxidation

In service environments, the components of C/SiC composite materials will react with oxidizing atmospheres, such as oxygen and water vapor, transforming the C fibers and SiC matrix from a solid state to a gaseous or liquid state. In these reactions, the main load-bearing phase, C fibers, will react with oxygen and gradually decompose into gaseous CO and CO_2, greatly weakening the load-bearing capacity of the C fibers, which is a key factor leading to the decrease in the macroscopic strength of the material. At the same time, the SiC matrix will also react with water vapor at high temperatures, generating molten SiO_2. In this paper, due to the low content of water vapor (only 5%), it will preferentially react with the SiC matrix and be consumed in large quantities; moreover, the by-products (CO and H_2) generated by the SiC reaction will inhibit the reaction process between C fibers and water vapor[18, 19]. In addition, multiple studies [20-24] have confirmed that, in a water-oxygen-coupled environment, oxygen is the primary factor determining the macroscopic failure of the carbon phase. Based on the above reasons, the reaction between the carbon phase and water vapor is not considered in this study.

During the stress oxidation stage, the oxidizing gas first diffuses into the material through prepared defects (coating cracks). It reacts with the carbon phase in the C/SiC composite materials, converting solid carbon fibers into gas. These reaction products escape through the coating cracks via gas diffusion. When external stress P is applied to the material, the coating cracks are pulled apart by tensile stress, providing a pathway for the oxidizing gas to enter the material interior. As the reaction

progresses, some carbon fibers degrade through oxidation, leading to additional cracks, while external stress further widens the coating cracks. The expansion of cracks enables the oxidizing gas to diffuse more rapidly into the internal area, accelerating the degradation process of carbon fibers. With the continuous effects of oxidation and external stress, more carbon fibers are oxidized or stretched and fractured, and the crack expansion and gas diffusion continue to intensify, ultimately leading to the fracture failure of C/SiC composite materials. In this process, the width of coating cracks is affected by external stress. At the same time, the diffusion of oxidizing gas and the degradation of carbon fibers mutually promote each other, forming a vicious cycle that ultimately exacerbates material failure.

During the oxidation of gases entering the interior of materials, the influence of their diffusion mechanisms must be considered. Different diffusion mechanisms yield different diffusion coefficients. In the oxidation process, differences in diffusion coefficients yield different oxidation rates. In this article, the relationship between the molecular mean free path λ of the oxidizing atmosphere and the oxidation channel e needs to be considered.

When $e \geqslant 100\lambda$, it is Fick diffusion, where collisions mainly occur between gas molecules as they pass through the pores, with fewer collisions between gas molecules and the pores. The effective diffusion coefficient is represented by D_F :

$$D_F = \frac{5.9543\times10^{-24}\times\left[\left(1/M_A\right)+\left(1/M_B\right)\right]^{1/2}T^{3/2}}{P\sigma_{AB}^2\Omega_{AB}} \tag{1}$$

When $e \leq 100\lambda$, it is Knudsen diffusion, where collisions between gas molecules are secondary, and the dominant factor is the collision between gas molecules and the pores. Its effective diffusion coefficient is represented by D_K :

$$D_K = \frac{2}{3}\left(\frac{8RT}{\pi M}\right)^{1/2} d \tag{2}$$

In these two equations, R is the ideal gas constant with a magnitude of $8.314\mathrm{J/mol\bullet K}$, M is the molar mass of the gas, P is the total pressure, σ is the collision diameter, and Ω is the collision integral, in the present condition:

$$D_F = 0.00506\sqrt[3]{T} \tag{3}$$

$$D_K = 17148\sqrt{T}\bullet d \tag{4}$$

If $0.1\lambda<e<100\lambda$, the diffusion coefficient can be expressed by[25, 26]

$$D^{-1} = D_F{}^{-1} + D_K{}^{-1} \tag{5}$$

For the reaction process between C Phase and oxygen, the oxidation process in the microscopic oxidation region can be simplified as follows: a series of processes in which oxygen reaches the reaction interface through a diffusion channel of a certain length and undergoes oxidation reaction, as shown in *Figure 4*. e represents the crack width, ς_0 represents the thickness of the SiC coating, and ς represents the distance traveled by the oxidizing gas diffusing to the internal Phase C reaction interface.

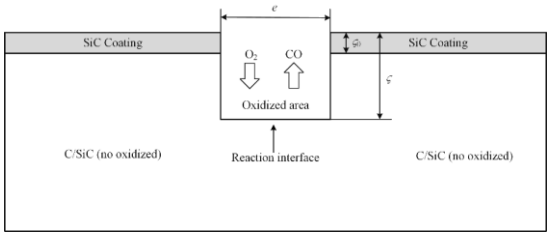


Figure 4 Stress oxidation damage mathematical model

The following assumptions are made when deriving the stress oxidation damage law: (1) the plain-weave C/SiC composite material consists of an external SiC coating and an internal C/SiC, with the internal SiC matrix and C fibers (including the PyC interfacial layer) uniformly mixed; (2) the oxidation process is quasi-steady state; (3) the reaction gas diffuses only through the gas phase to the internal reaction interface; (4) the influence of the boundary layer on gas diffusion is not considered; (5) the C-O_2 reaction is a first-order reaction, and CO is the main oxidation reaction product; (6) the reaction between SiC and O2 does not affect the O_2 concentration gradient.[27]

Based on the law of conservation of mass and the diffusion flux equation of oxygen in the CO-O_2 binary system, combined with the reaction stoichiometry and diffusion control approximation, MEI[27, 28] ultimately derived the relationship between crack propagation length and time through the integral relationship between carbon consumption rate and mass change:

$$\zeta = \left[\frac{4\bar{D}PM}{\rho_C RT} \ln(1+\chi_0)t + \zeta_0^{\,2} \right]^{\frac{1}{2}} \tag{6}$$

Where $\bar{D}$ is the effective diffusion coefficient (m^2/s), P is the total gas pressure (Pa), *M* is the molar mass of carbon (g/mol), ρ_C is the mass density of carbon fibers (g/m3), *R* is the gas content (J/mol·K), *T* is the absolute temperature (K), χ_0 is the mole fraction of oxygen in the inlet atmosphere.

In the finite element analysis of stress oxidation, we have set an oxidation damage variable ***d*** for the fiber bundle element. The oxidation depth determines the extent of damage to the fiber bundle element. When the oxidation depth is less than the position of the upper surface of the element in the oxidation direction, it is considered that the element has not been oxidized, and the damage variable is set to 0. When the oxidation depth is greater than the position of the lower surface of the element in the oxidation direction, it is considered that the element has been completely oxidized, and the damage variable is set to 1. For elements in the process of oxidation, the damage variable is set according to the following formula:

$$d = \frac{\varsigma - \varsigma_0(i)}{L^e(i)} \tag{7}$$

Where $L^e(i)$ represents the element length of fiber bundle element *i* in the oxidation direction, and $\varsigma_0(i)$ denotes the distance from the coating to the upper surface of the fiber bundle element in the oxidation direction.

Oxidative damage is represented by reducing the modulus, which is determined by the following formula:

$$\begin{aligned} E_f &= E_f^0(1-D_{oxidized}) \\ G_f &= G_f^0(1-D_{oxidized}) \end{aligned} \tag{8}$$

Where E_f and G_f represent the Young's modulus and shear modulus of the fiber bundle during the oxidation process, respectively, and E_f^0 and G_f^0 represent the initial Young's modulus and shear modulus of the fiber bundle.

Based on the principle of equal strain, the external tensile load *P*, was distributed on the elements on the side plane of the RVE model. The load allocated to each element was determined as follows. Define the modulus matrix of C/SiC to be

$$E = \left[E_1, E_{2/3}, E_m\right] \tag{9}$$

Where E_1 and $E_{2/3}$ are the longitudinal and transverse modulus of the fiber bundle, respectively, E_m is the modulus of the SiC matrix. The equivalent modulus E_t is:

$$E_t = E \times \Delta^T \tag{10}$$

Where Δ is the volume fraction vector of the longitudinal fiber bundles, transverse fiber bundles, and SiC matrix.

Thus, the average strain of C/SiC under constant tensile stress σ was obtained by:

$$\varepsilon = \frac{\sigma}{E_t} \tag{11}$$

Finally, the stress vector σ_d applied to the longitudinal fiber bundles, transverse fiber bundles, and SiC matrix is derived by

$$\sigma_d = \varepsilon \times E \tag{12}$$

Where $\sigma_d = \left[\sigma_1, \sigma_{2/3}, \sigma_{\mathrm{m}}\right]$, By using the above equation, the externally applied loads can be converted into stresses applied between different material properties, i.e., the stresses applied in the axial direction of the fiber bundle σ_1 , the stresses applied in the radial direction of the fiber bundle $\sigma_{2/3}$. The stresses in the matrix σ_{m} , and the application of the above stresses to the elements with different material properties constitute the loading conditions of the material.

In the boundary condition setting of the finite element model, we restored the loaded environment in the test condition to make it consistent with the equivalent simulation environment test situation, i.e., the situation when the specimen is subjected to tensile load in the INSTRON testing machine, where the upper and lower surfaces of the left end of the specimen are solidly supported. The upper and lower surfaces of the right end are subjected to the tensile load along the direction of the inside of the specimen face, as shown in *Figure 5*.

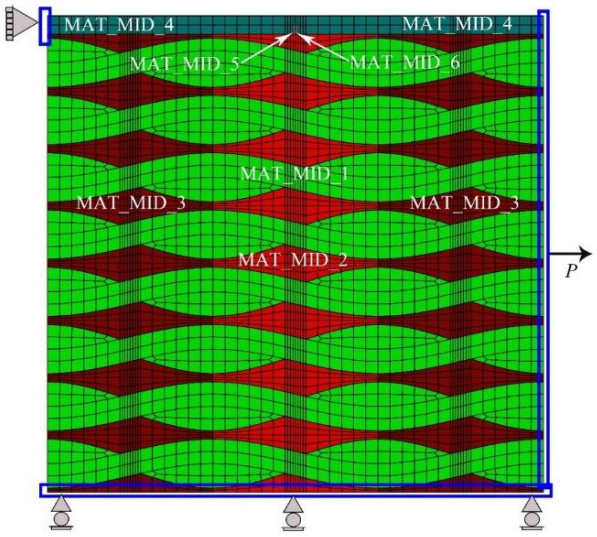


Figure 5 Material definition, boundary condition, and external load in the FEA model.

The SiC matrix and coating elements have isotropic mechanical properties, so using the Von Mises failure criterion determines the failure of the mechanical properties of the elements. The fiber bundle elements have orthotropic anisotropy in their mechanical properties, so it is more appropriate to use the Tsai-Hill failure criterion. Their elastic constants and thermal expansion coefficients are listed in

Table 1, respectively. Moreover, oxidation failure of the fiber bundle elements was considered by introducing an oxidation damage model.

Table 1 Constituent properties[29-31]

Constituent	Parameter	Value
Fiber bundle	Density ρ	1.84 g/cm^3
	Longitude tensile modulus E_{11}	163.6 GPa
	Transverse tensile modulus E_{22}/E_{33}	9.6 GPa
	Longitude shear modulus G_{12}	6.4 GPa
	Transverse shear modulus G_{13}/G_{23}	3.92 GPa
	Longitude Poisson's ratio v_{12}	0.20
	Transverse Poisson's ratio v_{13}/v_{23}	0.25
	Longitudinal coefficient of thermal expansion α_{11}	0.86×10^{-6}/K
	Transverse coefficient of thermal expansion α_{22}/α_{33}	6.63×10^{-6}/K
SiC Matrix	Density ρ	3.2 g/cm^3
	Tensile modulus E	350 GPa
	Shear modulus G	146 GPa
	Poisson's ratio v	0.17
	Coefficient of thermal expansion α	4.5×10^{-6} /K

In the numerical simulation of stress oxidation strength, the simulation process can be divided into two main stages: the stressed oxidation damage stage and the residual strength stage. In the stressed oxidation-damage stage, the temperature is first raised from the initial temperature to the working temperature. Subsequently, an external load is gradually applied until it reaches the working load P_1. Finally, the working load P_1 and operating temperature T_u are maintained until the specified oxidation time t_n is reached. The temperature and external load application methods for the stress-oxidation damage stage are shown in Eq. 13 and Eq. 14:

$$T=\begin{cases}1000 & t=0s\\ (T_u-1000)\times t\times10^5+1000 & 0<t<10^4 s\\ T_u & 10^4\le t\le10^6 s\end{cases} \tag{13}$$

$$P=\begin{cases}0 & 0s\le t\le10^4 s\\ P_1(t\times10^{-4}-1) & 10^4 s<t<2\times10^4 s\\ P_1 & 2\times10^4 s\le t\le t_n\end{cases} \tag{14}$$

Where t represents the loading time, and T_u and P_m stand for the service temperature and external service load, respectively.

2.3 Residual Strength

During the stress-oxidation stage, the fiber bundle element accumulates damage resulting from the coupling of mechanical and oxidative processes. The oxidation depth determines the oxidative damage variable d according to Eq. (7). The element stiffness is reduced according to Eq. (8). When d = 1 or the element satisfies the mechanical failure criterion (the Tsai-Hill criterion for the fiber bundle and the Von Mises criterion for the SiC matrix/coating), the element is removed. After the preset oxidation time has elapsed, the simulation proceeds to the residual-strength stage. In this stage, the working temperature T_u remains constant, and the external load is increased at a constant loading rate $\dot{P}$ until macroscopic failure occurs.

The loading scheme is shown in the following equation:

$$P=P_1+\dot{P}(t-t_n) \tag{15}$$

For the overall macroscopic failure criterion of the material, the failure cross-section element ratio method is employed to determine:

$$\beta = 1 - \frac{p}{\sigma_0} \tag{16}$$

Where β represents the proportion of the cross-section of the failed element, σ_0 denotes the strength of the material at the service temperature, and p signifies the external load during service. During the numerical simulation process, if the overall failure criterion is met, the material is deemed to have macroscopic failure.

Using ABAQUS/Explicit to analyze the residual strength of materials under high-temperature stress oxidation, failure criteria and oxidation damage variables are introduced via the VUMAT user subroutine interface. For each element property, material mechanical properties are assigned using user-defined variables, and element-level and global failure criteria are programmed. For the material subroutine MAT_MID_1, its primary function is to construct the stiffness matrix of the current element for the current increment step based on input parameters, calculate the stress tensor, strain tensor, and equivalent stress, and use the element failure criterion in conjunction with the oxidation failure criterion to perform stiffness degradation and determine element failure. Three state variables are defined: one to mark the element for deletion, one to record the element's characteristic length, and one to record the element number. When the element's stress satisfies the material element failure criterion or the oxidation failure criterion, the element is marked for deletion. If the current element satisfies the global failure criterion, the entire finite element calculation process stops, outputs the external load at that point, and calculates the residual strength. Subroutines for other materials are similar to MAT_MID_1; for the matrix subroutine, only mechanical property calculations and mechanical failure criterion assessments were performed.

3. Results and Discussion

According to the aforementioned simulation process, numerical simulations of the residual strength under stress-oxidation conditions were performed. In previous work, we selected the same materials used in the simulation and conducted stress oxidation experiments under identical conditions [17]. *Figure 6* and *Figure 7*, respectively, show the experimental and simulated residual strength values for different oxidation times under the same external load at different temperatures, and under the same temperature with different external loads. As shown in the figure, the error between the simulated and experimental strengths is greatest at an applied load of 140 MPa, a temperature of 900°C, and an oxidation time of 3500 s, reaching approximately 17%. This error falls within a reasonable range; the reason may be that the model assumes a uniform mixture of carbon fibers and the SiC matrix within the fiber bundle, thereby neglecting the preferential oxidation effect at the interface between the carbon fibers and the SiC matrix. Experimental observations indicate that the oxidation rate of PyC in the interfacial layer is higher than that of the carbon fiber matrix, leading to interfacial delamination and accelerated crack propagation.

Additionally, the model's assumptions about the multiscale reaction kinetics of oxidation lead to discrepancies between the predicted and experimental results at certain reaction temperatures. As shown in the contour plots, at higher temperatures, the crack length at the end of oxidation increases significantly compared to lower temperatures. Higher temperature accelerates the oxidation reaction, and longer oxidation time further enhances oxidation of the carbon fibers, leading to an accelerated fracture rate. This method effectively simulates the mechanical behavior of the residual strength of ceramic matrix composites under stress oxidation.

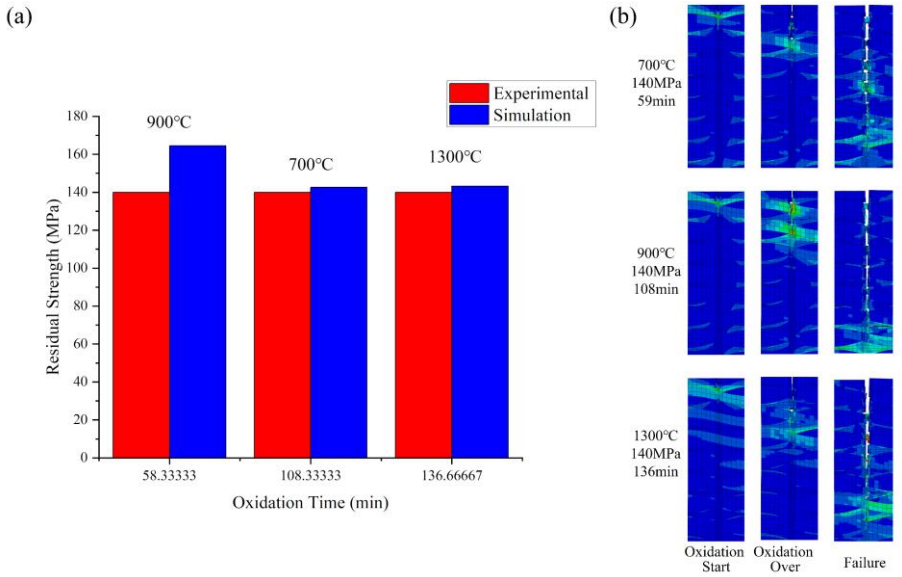


Figure 6 (a) Experimental and simulated results at 140 MPa; (b) Simulated stress contour plot

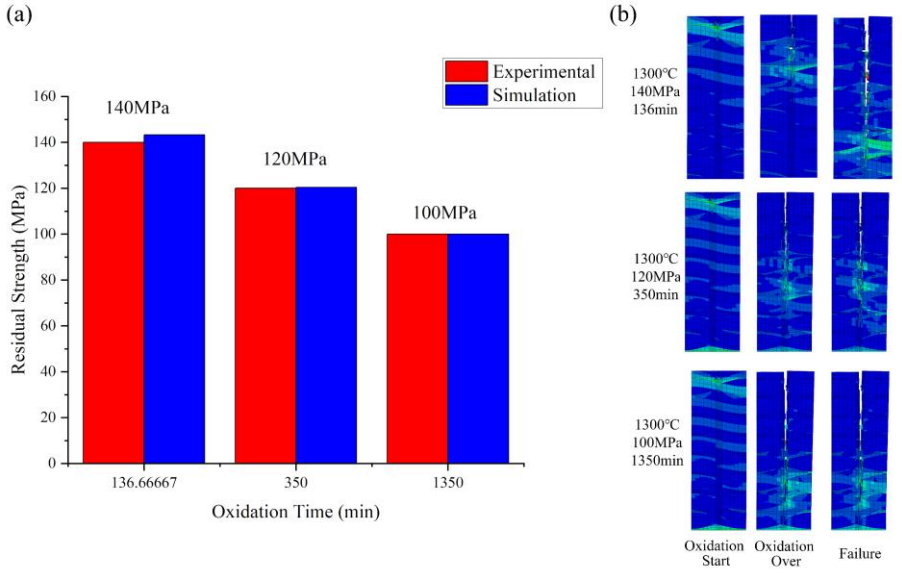


Figure 7 (a)Experimental and simulated results at 1300°C; (b)Simulated stress contour plot

3.1 Effect of Oxidation Time and Loads

Figure 8 (a) shows the relationship between residual strength and oxidation time at a service temperature of 1300°C under external loads of 100 MPa and 120 MPa. *Figure 8 (b)* presents stress contour plots of the simulation results for different oxidation times. The results indicate that at 1300°C, the material's residual strength decreases with increasing oxidation time. The oxidation time at which the residual strength drops to the level of the external load is taken as a reference and regarded as the "final failure time." Within the range where the oxidation time is less than 50% of the final failure time, the oxidative effect is weak, the fibers sustain minimal oxidative damage, the residual strength of the material remains high, and it exhibits good mechanical properties; When the oxidation time falls within the range of 50%–70% of the final failure time, the material's residual strength decreases slowly, exhibiting a "plateau phase"; after the oxidation time exceeds 70% of the final failure time, the material's residual strength drops rapidly, with pronounced oxidation effects, and the mechanical properties of the fibers decline significantly following oxidation. At shorter oxidation times, the relationship between the material's residual strength and the initial load is not pronounced. However, as oxidation time increases, the rate of decline in residual strength accelerates under higher loads. Combined with the material's long-term oxidation behavior, external loads and oxidation exhibit a significant synergistic effect. Higher stresses induce more or wider microcracks in the matrix, providing the necessary conditions for oxygen diffusion and thereby accelerating the oxidative degradation of carbon fibers.

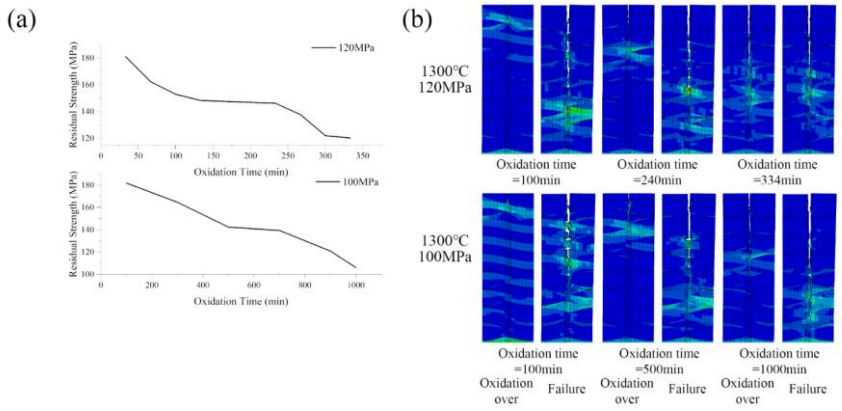


Figure 8 Results of simulations for different oxidation times:
(a) Simulation results; (b) Stress contour plot

3.2 Effect of temperature

Figure 9 shows the variation in residual strength of the material at different temperatures and oxidation times under a stress of 140 MPa. As oxidation time increases, the material's residual strength decreases at all temperatures. At lower temperatures, the residual strength declines slowly over shorter oxidation periods, and the oxidative effect on the carbon fibers is not significant; the primary cause of material failure is stress. However, after a prolonged oxidation period, the material's residual strength decreases significantly. This is because the oxidation of the carbon fibers becomes the dominant factor. At the same oxidation time, higher temperatures lead to a significant reduction in residual strength. This phenomenon is attributed to enhanced oxidation kinetics at high temperatures, which accelerate the depletion of carbon fiber bundles and lead to a rapid decline in load-bearing capacity.

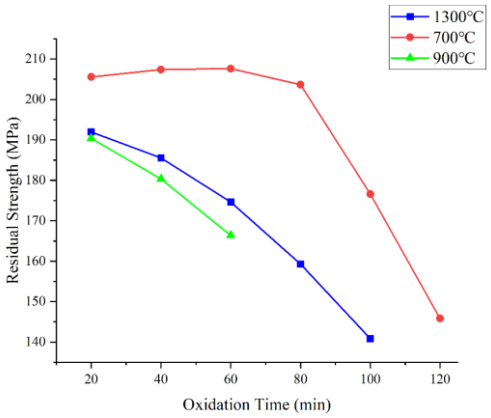


Figure 9 Simulation results of residual strength at 140 MPa under different temperatures

4. Conclusions

This study, based on the periodic structural characteristics of plain-woven C/SiC composites, extracted representative volume elements containing multi-layer weaving details and constructed a finite element analysis model that integrates chemical, thermal, and mechanical multi-field coupling effects. By introducing an oxidation-damage variable and combining the Tsai-Hill (fiber bundle) and Von Mises (matrix/coating) failure criteria, numerical simulations of the material's damage evolution and failure behavior under high-temperature stress-oxidation conditions were performed. The main conclusions are as follows:

1. The validity and reliability of the model were verified: The finite element simulation results showed good agreement with experimental data in terms of residual strength (120–160 MPa) and fracture life predictions, with a maximum error of approximately 17% (occurring under conditions of 140 MPa, 900°C, and 3500 s), which falls within an engineering-acceptable range. The errors primarily stem from the model's simplified assumption of homogeneous mixing between carbon fibers and the SiC matrix, as well as the neglect of the preferential oxidation effect at the interface layer (PyC); however, the model's overall effectiveness in predicting the stress-oxidation mechanical behavior of C/SiC composites has been confirmed.

2. Residual strength exhibits a three-stage degradation pattern with oxidation time: at a service temperature of 1300°C, the material's residual strength continuously decreases with prolonged oxidation time and can be divided into three stages: when the oxidation time is less than 50% of the final fracture time, oxidation damage is weak, and strength remains high (stable period); between 50% and 70%, residual strength slowly decreases, exhibiting a "plateau period"; when the oxidation time exceeds 70% of the final fracture time, carbon fiber oxidation leads to significant degradation of mechanical properties, and strength drops sharply (accelerated failure phase).

3. A significant synergistic damage mechanism exists between temperature and stress: an increase in temperature significantly accelerates the kinetics of oxidation reactions; under the same oxidation time, carbon fiber bundles degrade faster at high temperatures (e.g., 1300°C), resulting in a more pronounced decline in the material's load-bearing capacity; Meanwhile, external stress induces the propagation of microcracks in the matrix, providing pathways for oxygen diffusion, which further accelerates the oxidative degradation of carbon fibers, creating a vicious cycle of "crack propagation—oxygen ingress—fiber degradation—decrease in load-bearing capacity." During the low-temperature, short-duration oxidation phase, material failure is primarily stress-driven; after high-temperature, long-duration oxidation, carbon fiber oxidation becomes the dominant failure mechanism.

In summary, the multiscale finite element model established in this study can effectively predict the service life and residual strength of C/SiC composites under thermo-mechanical-oxidative coupling conditions, providing important theoretical foundations and numerical analysis tools for the oxidation-resistant design and reliability assessment of thermal structural materials for hypersonic vehicles. Future research may further optimize the model's description of oxidation behavior in the interfacial layer to improve prediction accuracy.

5. Contact Author Email Address

Yao Leijiang* , Professor, Yaolj@nwpu.edu.cn, corresponding autho

6. Copyright Statement

The authors confirm that they, and/or their company or organization, hold copyright on all of the original material included in this paper. The authors also confirm that they have obtained permission, from the copyright holder of any third party material included in this paper, to publish it as part of their paper. The authors confirm that they give permission, or have obtained permission from the copyright holder of this paper, for the publication and distribution of this paper as part of the ICAS proceedings or as individual off-prints from the proceedings.

References

[1] M. S. Park, J. Gu, H. Lee, S. H. Lee, L. Feng, and W. G. Fahrenholtz, "C/SiC Ceramic Matrix Composites with Extraordinary Thermomechanical Properties up to 2000 °C," (in English), *Nanomaterials,* vol. 14, no. 1, Jan 2024.

[2] X. P. Hu, Q. Liu, L. Chen, S. Liu, J. W. Guo, and W. Zhu, "Damage analysis of CVI SiCf/SiCm ceramic matrix composites under thermal shock," (in English), *International Journal of Fatigue,* vol. 194, May 2025.

[3] C. Zhang, P. Hu, L. C. Xun, Y. C. Zhou, J. C. Han, and X. H. Zhang, "A universal strategy towards the fabrication of ultra-high temperature ceramic matrix composites with outstanding mechanical properties and ablation resistance," (in English), *Composites Part B-Engineering,* vol. 280, Jul 1 2024.

[4] Z. W. Wang, Z. G. Dong, Y. C. Ran, R. K. Kang, and Y. Bao, "On understanding the mechanical properties and damage behavior of Cf/SiC composites by indentation method," (in English), *Journal of Materials Research and Technology-Jmr&T,* vol. 26, pp. 3784-3802, Sep-Oct 2023.

[5] R. Ranade, M. H. Hamza, L. Borkowski, and A. Chattopadhyay, "Analysis of damage mechanisms in fiber-reinforced ceramic matrix composites under thermomechanical loading at intermediate and high temperatures," (in English), *Journal of Composite Materials,* vol. 59, no. 22, pp. 2573-2590, Sep 2025.

[6] J. Huang, N. Yang, and H. M. Huang, "Oxidation and Sublimation Ablation of C/SiC Ceramics in Hypersonic Environments," (in English), *Journal of Spacecraft and Rockets,* Aug 15 2025.

[7] H. L. Ge *et al.*, "Comparative Ablation Behaviors of 2D Needled C/SiC and C/SiC-ZrC Composites," (in English), *Coatings,* vol. 14, no. 4, Apr 2024.

[8] Y. A. Shi, B. L. Zha, Q. D. Su, J. J. Wang, and S. Y. Li, "Thermal performance and ablation characteristics of C/C-SiC for thermal protection of hypersonic vehicle," (in English), *Journal of the European Ceramic Society,* vol. 41, no. 11, pp. 5427-5436, Sep 2021.

[9] M. C. Halbig, J. D. Mcguffin-Cawley, A. J. Eckel, and D. N. Brewer, "Oxidation kinetics and stress effects for the oxidation of continuous carbon fibers within a microcracked C/SiC ceramic matrix composite," (in English), *Journal of the American Ceramic Society,* vol. 91, no. 2, pp. 519-526, Feb 2008.

[10] M. Halbig and A. Eckel, "Oxidation of Continous Carbon Fibers Within a Silicon Carbide Matrix Under Stressed and Unstressed Conditions," 08/01 2000.

[11] X. Han *et al.*, "Tensile and stressed-oxidation behavior of 2D SiC/BN/SiC composites at Intermediate Temperatures in Air," (in English), *Ceramics International,* vol. 48, no. 1, pp. 1-9, Jan 1 2022.

[12] X. Han *et al.*, "Stressed-oxidation behavior of 2D CVI SiC/BN/SiC at elevated temperature in air," (in English), *Ceramics International,* vol. 47, no. 20, pp. 28158-28166, Oct 15 2021.

[13] Y. Meng, S. Yang, and X. Liu, "Investigation of the tensile mechanical properties and failure mechanisms of 2D SiC/SiC composites in thermal, mechanical, and oxidation environments," *Journal of Physics: Conference Series,* vol. 2955, no. 1, p. 012044, 2025/02/01 2025.

[14] L. Xi *et al.*, "Internal damage evolution of C/SiC composites in air at 1650 °C studied by in-situ synchrotron X-ray imaging," *Composites Part B: Engineering,* vol. 288, p. 111878, 2025/01/01/ 2025.

[15] H. Mei, "Modelling environmental effects on stress oxidation behaviour of carbon fiber reinforced ceramic matrix composites," (in English), *Advances in Applied Ceramics,* vol. 108, no. 2, pp. 123-127, Feb 2009.

[16] P. Chen, X. M. Niu, X. H. Chen, Z. G. Sun, P. J. Zou, and Y. D. Song, "Modeling the Failure Time and Residual Strength of C/SiC Composites under Stress-Oxidation Environment," (in English), *Transactions of the Indian Ceramic Society,* vol. 79, no. 4, pp. 212-220, Oct 1 2020.

[17] G. Q. Chen, L. J. Yao, L. J. Zhang, B. Li, and X. Y. Tong, "Numerical simulation on stress rupture life of C/SiC under wet oxygen condition," (in English), *Journal of the American Ceramic Society,* vol. 108, no. 9, Sep 2025.

[18] X. g. Luan, J. Zhang, and L. Cheng, "Effects of water vapor on corrosion behaviors of C/SiC in oxidizing atmosphere containing Na2SO4 vapor," *Composites Part B: Engineering,* vol. 43, no. 8, pp. 2968-2972, 2012/12/01/ 2012.

[19] X. Y. Liu, J. Zhang, L. T. Zhang, Y. D. Xu, and X. G. Luan, "Failure mechanism of C/SiC composites under stress in oxidizing environments," (in Chinese), *Journal of Inorganic Materials,* vol. 21, no. 5, pp. 1191-1196, Sep 2006.

[20] E. J. Opila, "Variation of the oxidation rate of silicon carbide with water-vapor pressure," (in English), *Journal of the American Ceramic Society,* vol. 82, no. 3, pp. 625-636, Mar 1999.

[21] C. E. Ramberg and W. L. Worrell, "Oxygen transport in silica at high temperatures: Implications of oxidation kinetics," (in English), *Journal of the American Ceramic Society,* vol. 84, no. 11, pp. 2607-2616, Nov 2001.

[22] R. C. Robinson and J. L. Smialek, "SiC recession caused by SiO scale volatility under combustion conditions:: I, experimental results and empirical model," (in English), *Journal of the American Ceramic Society,* vol. 82, no. 7, pp. 1817-1825, Jul 1999.

[23] K. L. More, P. F. Tortorelli, M. K. Ferber, and J. R. Keiser, "Observations of accelerated silicon carbide recession by oxidation at high water-vapor pressures," (in English), *Journal of the American Ceramic Society,* vol. 83, no. 1, pp. 211-213, Jan 2000.

[24] P. F. Tortorelli and K. L. More, "Effects of High Water-Vapor Pressure on Oxidation of Silicon Carbide at 1200°C," *Journal of the American Ceramic Society,* vol. 86, no. 8, pp. 1249-1255, 2003/08/01 2003.

[25] J. Szekely, J. W. Evans, and H. Y. Sohn, "Chapter 8 - Gas—Solid Reactions of Industrial Importance," in *Gas-solid Reactions*, J. Szekely, J. W. Evans, and H. Y. Sohn, Eds.: Academic Press, 1976, pp. 338-391.

[26] R. Krishna and J. M. van Baten, "Investigating the validity of the Bosanquet formula for estimation of diffusivities in mesopores," (in English), *Chemical Engineering Science,* vol. 69, no. 1, pp. 684-688, Feb 13 2012.

[27] J. J. Schichtel and A. Chattopadhyay, "Modeling the two-way coupling of stress, diffusion, and oxidation in heterogeneous CMC microstructures," (in English), *Journal of the European Ceramic Society,* vol. 43, no. 2, pp. 261-272, Feb 2023.

[28] M. H, "Damage evolutions and failure mechanisms of 2D C/SiC in coupled complex environments," doctor, Northwestern Polytechnical University, Xi'an, China, 2007.

[29] L. D. Chen, X. Y. Tong, L. J. Yao, Z. S. Li, and Y. Lv, "Microstructure Modeling and Further Effective Property Prediction for Plain Weave C/SiC Composites Considering Manufacturing Process," (in English), *Advanced Science Letters,* vol. 4, no. 4-5, pp. 1444-1449, Apr-May 2011.

[30] H. B. Wang, W. H. Zhang, Y. J. Xu, and Q. F. Zeng, "Numerical computing and experimental validation of effective elastic properties of 2D multilayered C/SiC composites," (in English), *Materials Science and Technology,* vol. 24, no. 11, pp. 1385-1398, Nov 2008.

[31] S. K. Mital, P. Murthy, and J. DiCarlo, "Characterizing the properties of a woven SiC/SiC composite," *Journal of Advanced Materials -Covina-,* vol. 35, pp. 52-58, 01/01 2003.